2016

Characterization of Photonic Waveguides Using Fourier Analysis

Sam Olson
Portland State University

Characterization of Photonic Waveguides Using Fourier Analysis

by

Sam Olson

An undergraduate honors thesis submitted in partial fulfillment of the

requirements for the degree of

Bachelor of Science

in

University Honors

and

Physics

Thesis Adviser

Dr. Rolf Könenkamp

Portland State University

2016

ABSTRACT

In this work, several characteristics of indium tin oxide (ITO) thin-film waveguides are analyzed. The simulation software COMSOL Multiphysics is used to create two waveguide models, one with a single 400 nm diameter hole, and one with two 400 nm diameter holes. A 410 nm light source is incident upon the models at an angle of 60° from the normal. Fourier analysis performed upon the normalized electric field at the surface led to effective indices in the waveguide of about 1.76 and 2.05.

ACKNOWLEDGMENTS

I would like to thank Dr. Rolf Könenkamp for allowing me to pursue this research through his lab at Portland State. When I first committed to completing my thesis through his lab, I had had only minimal experience in optics. Rolf showed astounding patience and shared an immense amount of his knowledge on the subject, without which I would have struggled greatly. I would also like to thank Dr. Robert C. Word for the sharing of his knowledge in optics as well as Fourier analysis and COMSOL. Lastly, I would like to thank Ph.D. candidate Theodore Stenmark for his time spent giving me feedback on drafts as well as tutoring me in COMSOL modeling.

Table of Contents

Table of Figures

Chapter 1 – Introduction

1.1 Background

This thesis focuses on the simulated behavior of light within modeled planar waveguides. Waveguides are quite self-descriptive. In simple terms, they are materials that are capable of guiding waves with minimal loss of energy. They are quite common in modern life due to their usefulness in communication, sensing, and energy transmission. Different types of waveguides are capable of transmitting energy in different dimensions, mainly depending upon their geometries.

The waveguides used in the research for this thesis are optical waveguides, which guide light waves in and around the optical (visible) spectrum of 400 nm to 700 nm. Specifically, planar waveguides were used in this research. The waveguides are constructed of three main "layers". The top layer is the air layer, where no material is present. The second layer is the dielectric layer. In this case the dielectric layer is made of indium tin oxide (ITO). The final layer is a borosilicate glass substrate. The light waves are trapped within the ITO layer by means of total internal reflection.

Optical waveguides have many uses in modern technology. One of the most innovative and ubiquitous uses of optical waveguides is in optical fibers. Optical fibers are capable of transmitting data over vast distances with minimal attenuation of energy, and have practically replaced all traditional wires for submarine communication cables [1]. Optical fibers use silicon dioxide (silica) as a waveguide. The silica must be free of even the smallest amounts of contamination to avoid loss of energy.

Optical waveguides also have quite a potential in the field of photonic circuits. These circuits aim to replace silicon-based circuit boards with optical waveguides. These waveguides would be able to mimic wires and transistors, using photons in lieu of electrons [2]. These photonic circuits are not inhibited by the Joule effect, whereas electrical conductors release heat when electrons pass through them. The absence of the Joule effect means far less overheating on chips. Another current use of waveguides is in the field of biosensors. Waveguides have been able to make biosensors smaller, allowing for more of them to be allocated onto a single chip [3].

The inspiration for this research comes mainly from the desire to find better ways of sensing and communicating using optical waveguides. With these small, relatively simple simulations, a lot of information about the materials' interactions with electromagnetic waves can be found.

1.2 Software

The images and data gathered for this experiment were obtained through a software suite called COMSOL Multiphysics. COMSOL is a simulation software that can be used for solving a multitude of different physics problems. The electromagnetic wave tools were used extensively for this project. COMSOL works by solving partial differential equations by approximation using the finite element method. Different levels of meshing give different levels of accuracy, at the cost of memory usage. A meshing size of about $\lambda/10$ (where λ is the incident wavelength) was used on the models, with finer meshing used around the holes and walls in the waveguide

(roughly $\lambda/20$). In addition to COMSOL, MATLAB was used for data analysis and plotting.

Chapter 2 – Theory

2.1 Waveguide Optics

Optical waveguides operate by way of total internal reflection [4]. Total internal reflection occurs when light is incident upon a transparent surface at an angle greater than the critical angle, θ_C, which is given by a rearrangement of Snell's law,

$$\theta_C = \sin^{-1}\frac{n_2}{n_1}\ , \qquad (1)$$

where n_1 is the index of refraction of the material that the wave is reflecting into, and n_2 is the exterior material. If the angle of incidence is below this critical angle, not all of the light will be reflected back into the material, and some amount of refraction will occur. If the angle is at or above the critical angle, the wave will bounce back and forth in a zigzag motion through the length of the waveguide.

Material	Index of Refraction	Critical angle at interface with ITO
Air	1	27.9°
ITO	2.14	-
Glass	1.52	45.3°

Table I: Optical properties of the waveguide materials for 400 nm light (indices of refraction given by COMSOL)

For the materials used in this experiment, the two critical angles that the light needed to meet for total internal reflection were 27.9° and 45.3° from the normal (Table I).

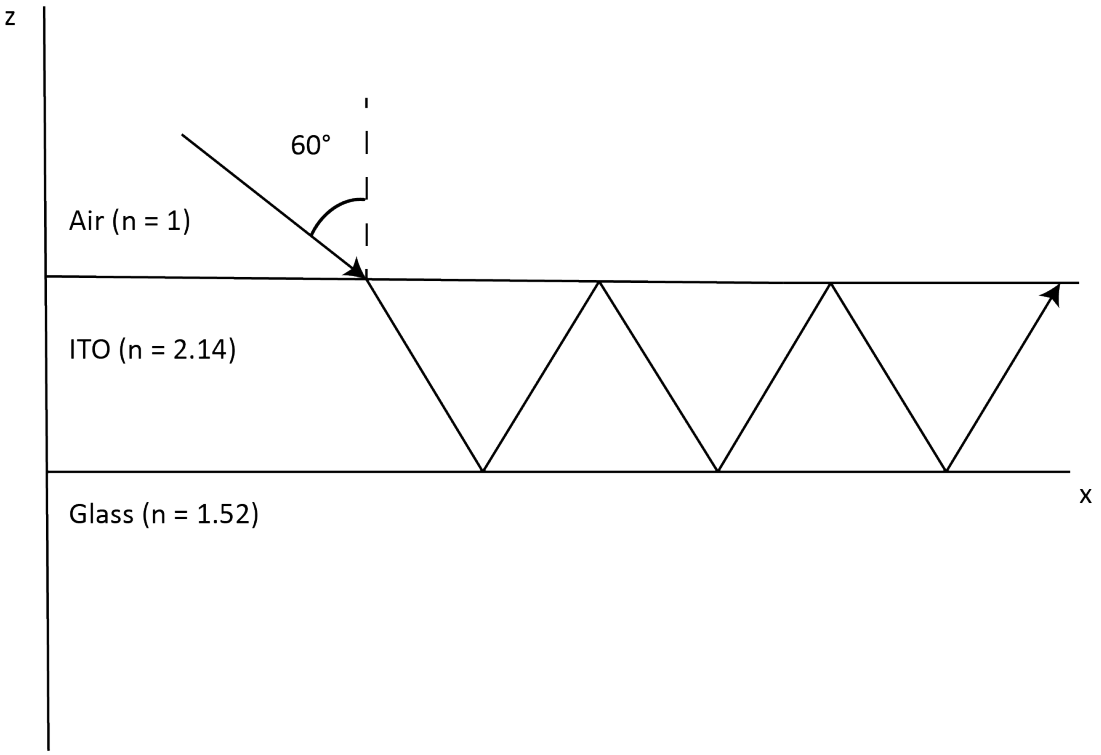

Figure I: The light in a waveguide travels in a zigzag motion across the depth of the dielectric ITO layer, with a monochromatic light source incident at an angle of 60° from the normal

2.2 Electromagnetic Waves

Visible light is a form of electromagnetic radiation (EMR). EMR is composed of electromagnetic waves, which contain both electric and magnetic fields. The fields are orthogonal to one another, and both fields are orthogonal to the direction of propagation.

Light confined to a waveguide is constricted to travelling only in certain modes. These modes are dependent upon the direction of polarization of the light. There can exist transverse electric (TE), transverse magnetic (TM), and transverse electromagnetic (TEM) polarizations. For example, TE modes occur when the electric field is perpendicular to the plane of incidence.

As with many problems in electromagnetics, to solve for the modes in a waveguide one must solve Maxwell's equations with a set of boundary conditions. A first simplification applicable for the case of waveguides is to assume the "source-free" version of Maxwell's equations. In the source-free version of Maxwell's equations there is no charge giving off electromagnetic radiation. In this state, Maxwell's equations are [5]:

$$\nabla \cdot \mathrm{E} = 0 \tag{2.1}$$

$$\nabla \cdot \mathrm{B} = 0 \tag{2.2}$$

$$\nabla \times \mathrm{E} + \frac{\partial \mathrm{B}}{\partial \mathrm{t}} = 0 \tag{2.3}$$

$$\nabla \times \mathrm{B} - \varepsilon\mu \frac{\partial \mathrm{E}}{\partial \mathrm{t}} = 0 \tag{2.4}$$

Where E is the electric field, B is the magnetic field, ε is the permittivity of free space, and μ is the permeability of free space. Equations (2.2) and (2.3) are unchanged from the standard Maxwell's equations. They state respectively that there are no magnetic monopoles, and that an electromotive force is created by magnetic flux. Equations (2.1) and (2.4) are slightly altered from the standard. Equation (2.1) is equated to zero due to an absence of charge (and thus no electric

flux). Equation (2.4) is missing the current density portion from the standard (due again to an absence of charge).

These forms of Maxwell's equations give rise to the electromagnetic wave equation. The modes of a waveguide are defined as the solutions to the electromagnetic wave equation [6],

$$\nabla^2 E = \frac{1}{c^2}\frac{\partial^2 E}{\partial t^2}, \tag{3}$$

where E is the electric field and c is the speed of light (≈3x10^8 m/s). This equation applies to electromagnetic waves in a vacuum, but since the environment of interest has a refractive index, and thus a lower propagation speed, the following equation is used,

$$\nabla^2 E = \frac{n^2}{c^2}\frac{\partial^2 E}{\partial t^2}, \tag{4}$$

where the relation $v = c / n$ has been used to replace c for an electromagnetic wave travelling with velocity v in a material of refractive index n. Solutions to this equation are exponentials of the form [6],

$$E(t) = E_0 e^{i\omega t}, \tag{5}$$

where E_0 is the base amplitude of the electric field, t is the time, and ω is the angular frequency of the wave.

2.3 Effective Index

An effective index is produced in a material when the phase of a wave changes over a certain distance. This leads to a change in the wavenumber. A smaller wavelength will produce a larger wavenumber. When a light wave is totally internally refracted

into a material, the phase is changed. The refractive index of the material dictates how big of a change this is. The change in phase leads to an observed "effective" index. This index is equivalent to [7],

$$n_{eff} = nsin\varphi \,, \tag{6}$$

where n_{eff} is the effective index of the material, n is the index of refraction of the material, and φ is the angle of incidence of the guided light in the waveguide.

2.4 Interference

As a wave, light is subject to both constructive and destructive interference. Interference occurs when two light waves interact. In the case of the waveguide, the light incident upon the waveguide that illuminates the entire surface, and the light coupled inside the waveguide through the holes, interfere with one another to produce a pattern. This pattern occurs throughout the three dimensional confines of the waveguide wherever the two beams overlap. In order to obtain a spatially constant interference pattern, the light beams must be coherent. This means that they must have a constant phase difference, as well as the same frequency.

The wavenumber (spatial frequency) of the incident wave is given by,

$$k = \frac{2\pi}{\lambda} \,, \tag{7}$$

where λ is the wavelength of the light. Since the light is incident at an angle θ and the interference pattern is observed in the surface plane, the component of the wave vector of the incident light parallel to the waveguide surface must be calculated. With simple trigonometry this gives,

$$k_{surf} = ksin\theta \ , \tag{8}$$

where k_{surf} is the wavenumber of the incident light in the surface plane. Inside the waveguide, the wavenumber is

$$k_{ITO} = kn_{eff} \ , \tag{9}$$

where k is the free space wavenumber, and n_{eff} is the effective index of the mode propagating inside the ITO layer.

The wavenumber of the resultant interference pattern of these waves (k_i) can be computed in general using vectors,

$$\boldsymbol{k}_i = \boldsymbol{k}_{\boldsymbol{ITO}} + \boldsymbol{k}_{\boldsymbol{surf}} . \tag{10}$$

Where the direction of the vectors is the direction of propagation of the light. When using equation (10) to analyze waves propagating in the positive direction (forward) in the waveguide, the plus becomes a minus due to the geometry of the incident wave [7],

$$k_i = kn_{eff} - ksin\theta \ . \tag{11}$$

When (10) is used to analyze waves propagating in the negative direction (backward), the plus sign is maintained,

$$k_i = kn_{eff} + ksin\theta \ . \tag{12}$$

2.5 Fourier Transform

The Fourier transform is extremely useful for studying the components of periodic functions. By taking the Fourier transform, a set of data can be converted to a domain based on frequency instead of time (or spatial frequency instead of

distance). The Fourier transform works by matching a summation of periodic functions to a set of data [9],

$$F(k) = \int_{-\infty}^{\infty} f(x)e^{ikx}dx, \quad (13)$$

where *F(k)* represents the Fourier transform in the spatial frequency domain, *f(x)* is the function in the spatial domain, and *k* is the spatial frequency. In the context of waveguides, this spatial frequency Fourier transform comes in quite handy. When a data set is transformed using Fourier analysis, the result is a two dimensional paired data set. One dimension of the data set contains an ordered array of "sample" numbers, and the other contains the relative strengths of each frequency. If *N* data points are analyzed, the sample number array will consist of the data set *1, 2, 3, … , N*. When this data set is plotted, the peaks represent the frequencies that are most prevalent in the sample.

Chapter 3 – Experimental Process

Two different models were made for use in this research. Both models were based on a rectangular box with a width (x-axis) of 4 μm, and a height (y-axis) of 2 μm. The thickness (z-axis) of the ITO layer within which the light propagates is 250 nm. The first model to be analyzed contains a single 400 nm diameter hole, offset from the middle of the XY plane by 900 nm on the x-axis. The second model contains two 400 nm diameter holes, also offset on the x-axis by 900 nm. The distance between the centers of the two holes is 800 nm.

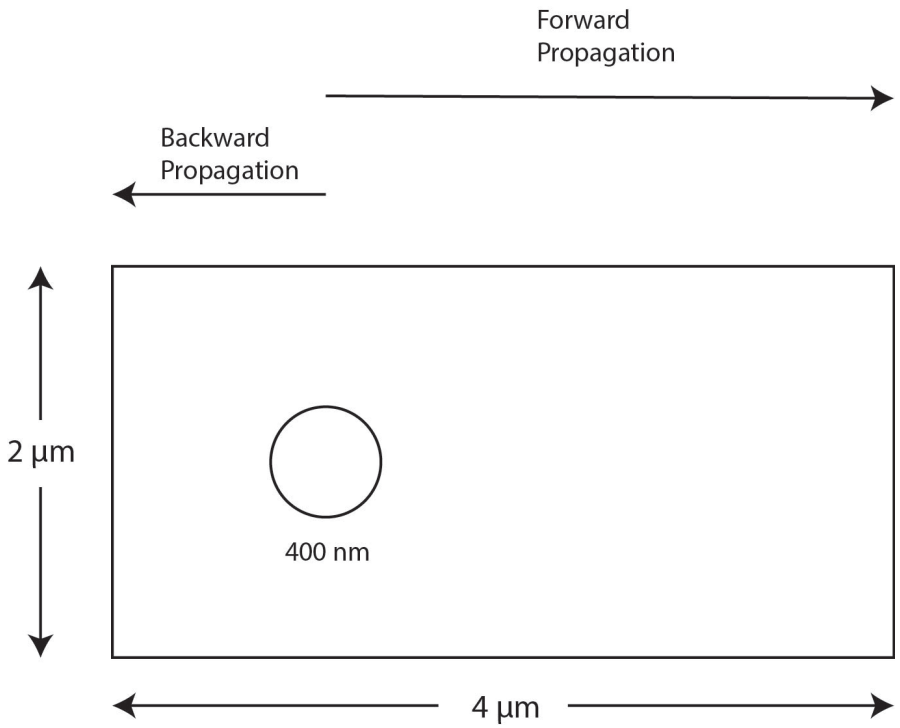

Figure II: Basic dimensions of the first model, with propagation directions labeled. The second model has identical dimensions, save for the addition of another 400 nm hole.

The light wave is TE polarized and is incident upon the waveguide at an angle of 60° from the normal. The wave is allowed to couple into the waveguide through the hole, or holes, in the ITO layer. Data concerning the time averaged electric field versus the distance along the x-axis was extracted and analyzed.

Chapter 4 – Data and Analysis

4.1 Single 400 nm hole

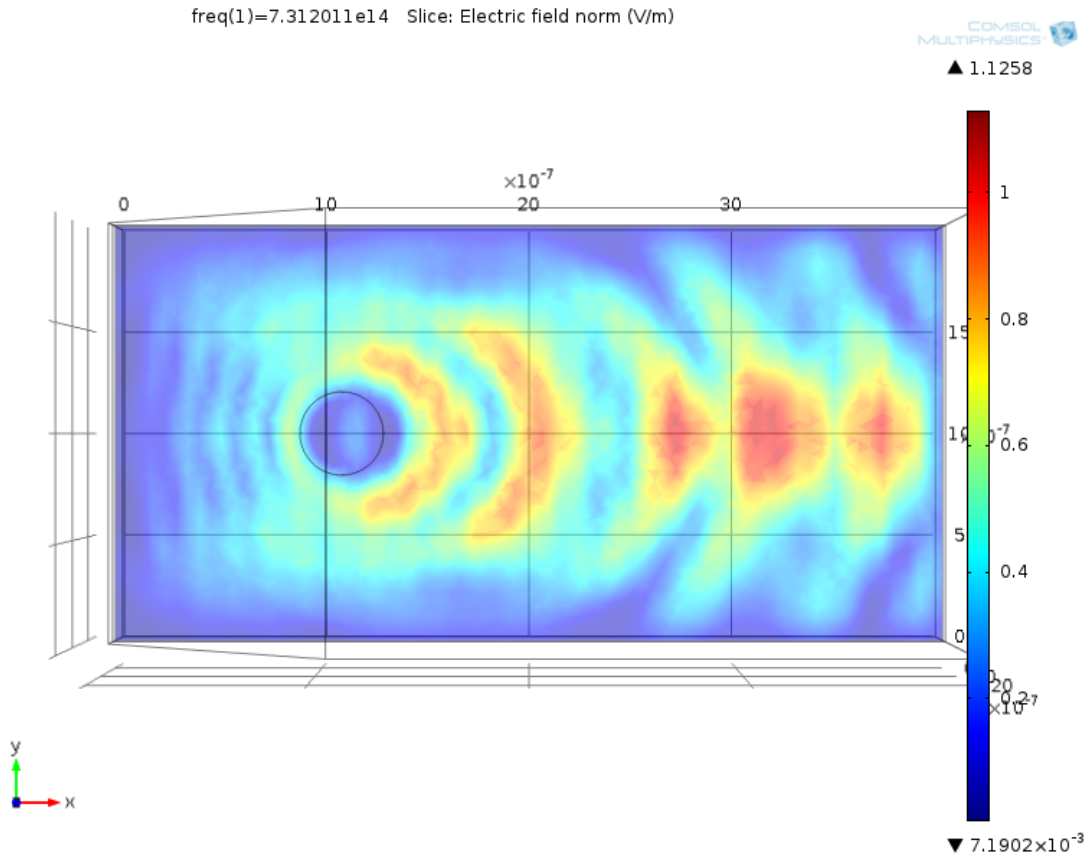

Figure III: Face down view of the waveguide with a single 400 nm diameter hole. Distance units are in tenths of micrometers (or $1x10^{-7}$ m)

Figure III above shows the time averaged electric field at the surface of the waveguide. The red portions of the graph represent the maxima of the interference pattern, while the blue portions represent minima. Some backscattering is evident from the small perturbations of electric field behind the hole. As the incident light strikes the circular hole in the ITO, each point along the circumference of the hole acts as a point source, and light propagates outward radially. There also seems to be

a small amount of light reflecting back off of the walls. This is due to imperfections in the absorption of the model.

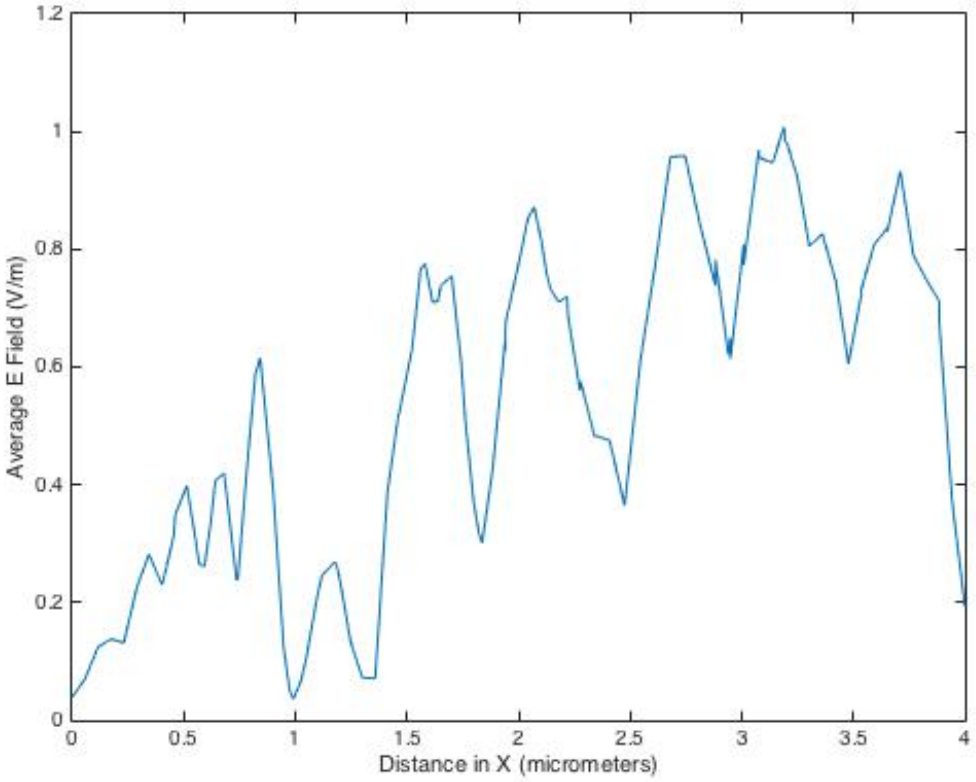

Figure IV: A plot of the average electric field parallel to the z-axis in volts per meter versus the distance along the length of the waveguide (x-axis) in micrometers for a single hole

Figure IV shows how the electric field interference is distributed across the length of the waveguide. The slice is taken straight along the middle of the y-axis down the entire 4 μm length of the waveguide. The major dip between 0.9 μm and 1.3 μm is due to the hole in the ITO.

4.2 Two 400 nm Holes

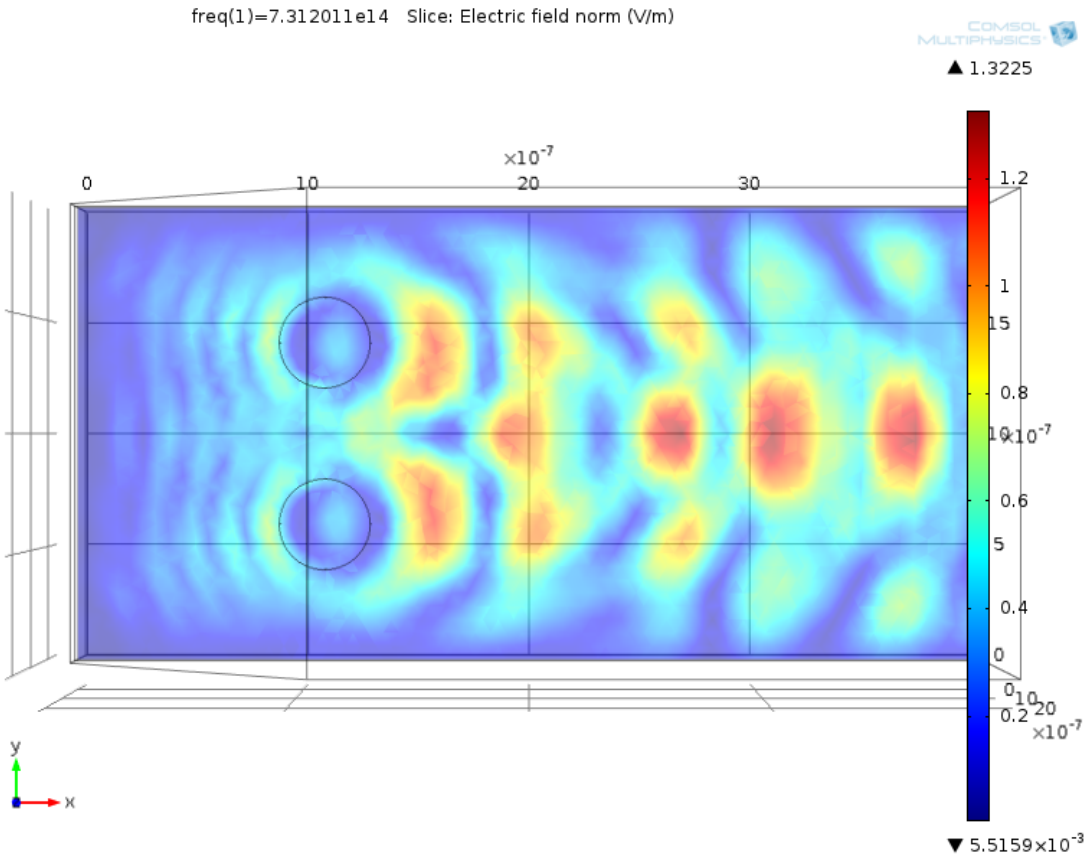

Figure V: Face down view of the waveguide with two 400 nm diameter holes Distance units are in tenths of micrometers (or $1x10^{-7}$ m)

Figure V shows the XY plane of the waveguide with the interference pattern for the two-hole set up. The resulting pattern is strikingly different from the single hole. This is, of course, due to a lateral interference between the waves originating from the two holes. Now, the light in the waveguide not only experiences interference with the incident light from outside the waveguide, but it also experiences interference with the light that was coupled in from the opposite hole.

Again, there is some level of backscattering from the holes. This time the scattering seems to be in two more distinct wave fronts – one for each hole.

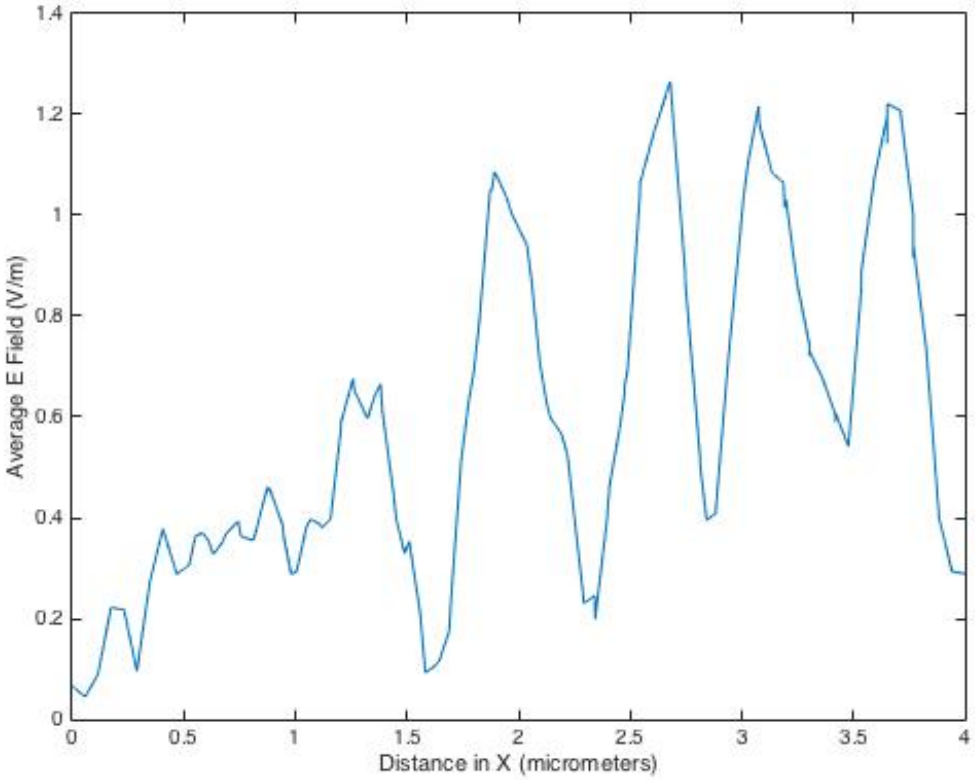

Figure VI: A plot of the average electric field parallel to the z-axis in volts per meter versus the distance along the length of the waveguide (x-axis) in micrometers for two holes

Figure VI shows the data for the electric field strength across the waveguide for the two hole model. Note that there is not as significant of a dip in the electric field length where the holes are located (between 0.9 μm and 1.3 μm). This is of course due to the fact that the middle of the y-axis at that length is now filled with ITO instead of air. Note also the larger amplitudes of the maxima and minima. This is due to the added constructive and destructive interference of the second hole.

4.3 Fourier Analysis of Data

4.3.1 Methods of Analysis

In order to find the spatial frequencies, and subsequently wavelengths, of the interference pattern, MATLAB's Fast Fourier Transform (FFT) function was used. The FFT function takes the input data, and does a fast Fourier transform algorithm on it to transform it into the frequency domain. In order to get the purest results, the analysis of each waveguide was separated into the distance to the left of the hole (backward), and the distance to the right of the hole (forward). The difference of the interference patterns in the two directions is due to the fact that the interference from the backscattered light causes a pattern with a drastically diminished wavelength when compared to the interference wavelengths further past the holes. This can also be seen numerically with the differences between equations (11) and (12).

MATLAB's FFT function effectively takes the data array, and applies the FFT algorithm to it. In doing so, it creates a mirrored, symmetric plot that has as many samples as data points that were provided to it. Therefore, the following figures only contain the left hand side of the data, as including the mirrored version would be redundant and confusing when making calculations. In order to obtain the appropriate interference frequencies, f_I, it is necessary to use the following method,

$$f_i = \frac{x * f_{samp}}{N}, \tag{14}$$

where x is the sample number, f_{samp} is the sampling frequency (in μm^{-1}), and N is the number of data points given to the FFT function. This is simply a method of scaling the data. The COMSOL models were created with f_{samp} = 32 μm^{-1}. The number of data

points was 28 for the backwards direction of the single hole model, 91 for the forwards direction of the single hole model, 30 for the backwards direction of the dual hole model, and 107 for the forwards direction of the dual hole model.

It is quite straightforward from here to find the wavelength. All one must do is apply the following simple equation to obtain the interference wavelength,

$$\lambda_i = \frac{1}{f_i}. \tag{15}$$

4.3.2 Single Hole Model

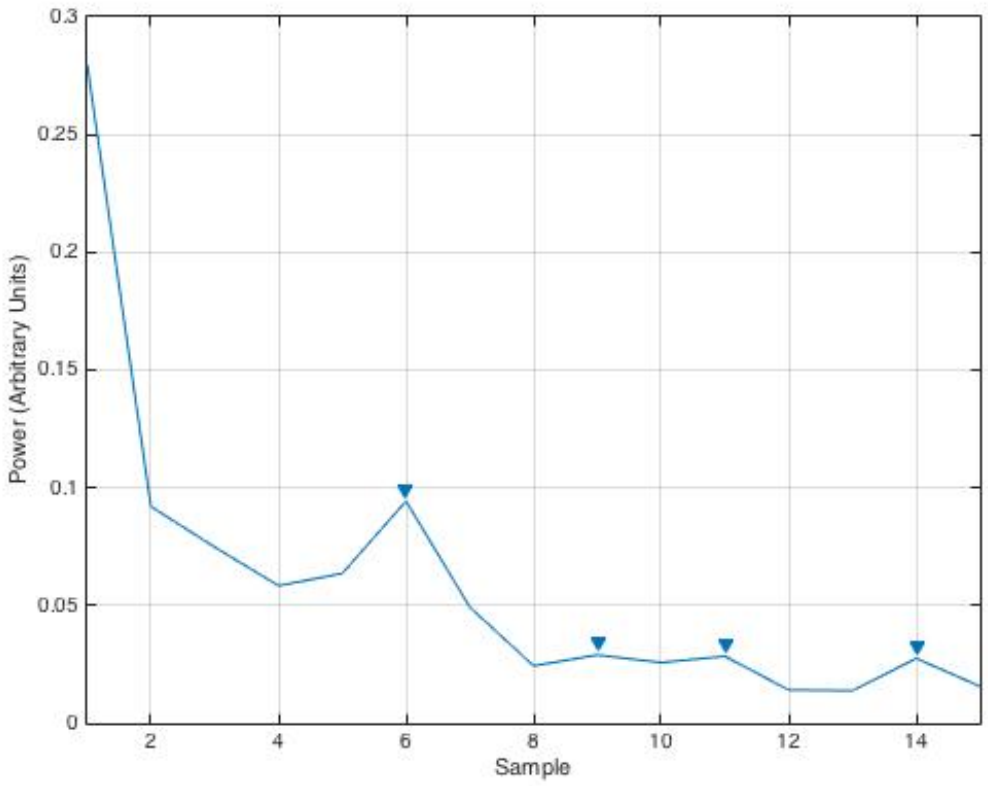

Figure VII: The FFT of the area behind the single hole in the ITO layer (0 μm to 0.9 μm)

In figure VII, there is one clear prominent peak at sample number 6 and several lesser peaks. These peaks were labeled automatically by MATLAB's *findpeaks* function. Applying equation (13), the peak at sample number 6 gives an interference frequency of 7.07 μm^{-1}. Inverting this number gives 141 nm. This is the interference pattern wavelength that is seen in figure III to the left of the hole.

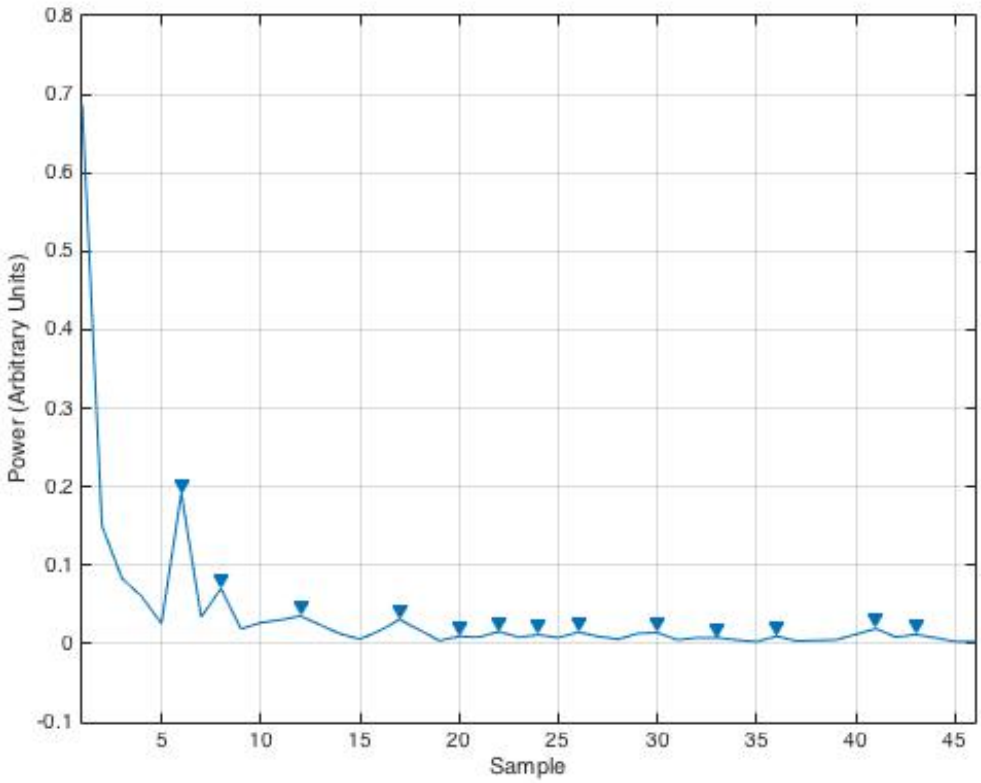

Figure VIII: FFT of the area forward from the single hole in the ITO layer (1.3 μm to 4 μm)

In figure VIII, there is one very prominent peak and one slightly less prominent peak. These peaks occur at sample numbers 6 and 8. This leads to interference frequencies of 2.18 μm^{-1} and 2.90 μm^{-1} respectively, with corresponding

wavelengths of 460 nm and 344 nm. This represents the interference pattern seen to the right of the hole in figure III.

4.3.3 Two Hole Model

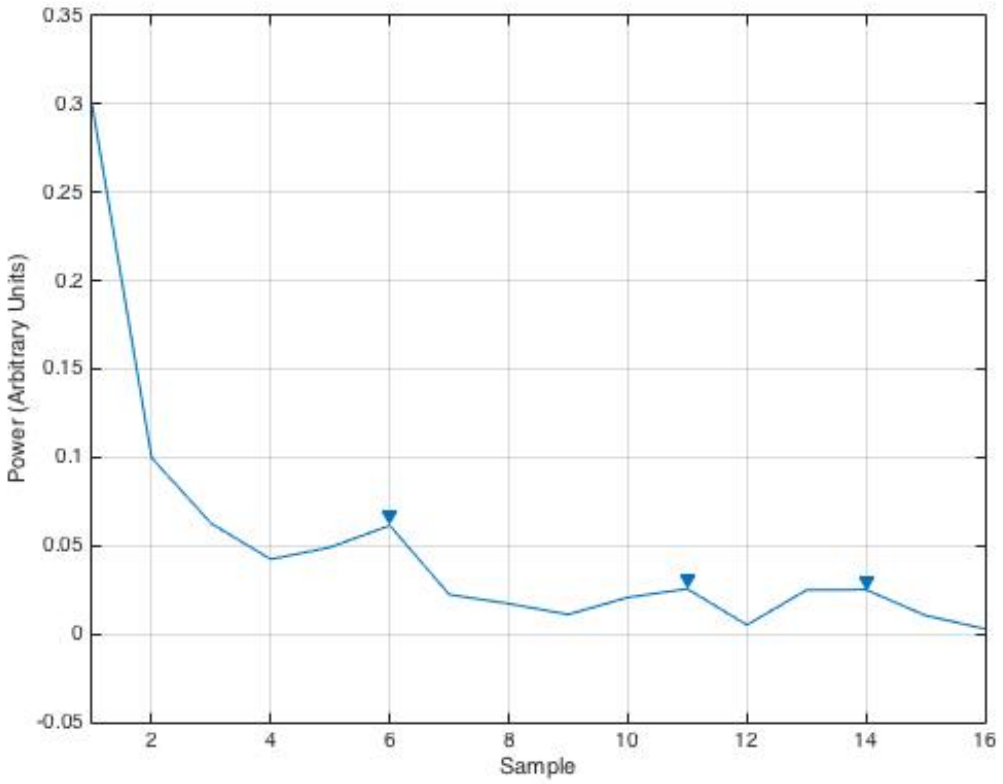

Figure IX: FFT of the area behind the two holes in the ITO layer (0 μm to 0.9 μm)

In figure IX there is one clear peak that rises above the others, occurring at sample number 6. This gives an interference frequency of 6.60 μm^{-1}, and a corresponding wavelength of 152 nm. This represents the interference pattern seen to the left of the two holes in the model in figure V.

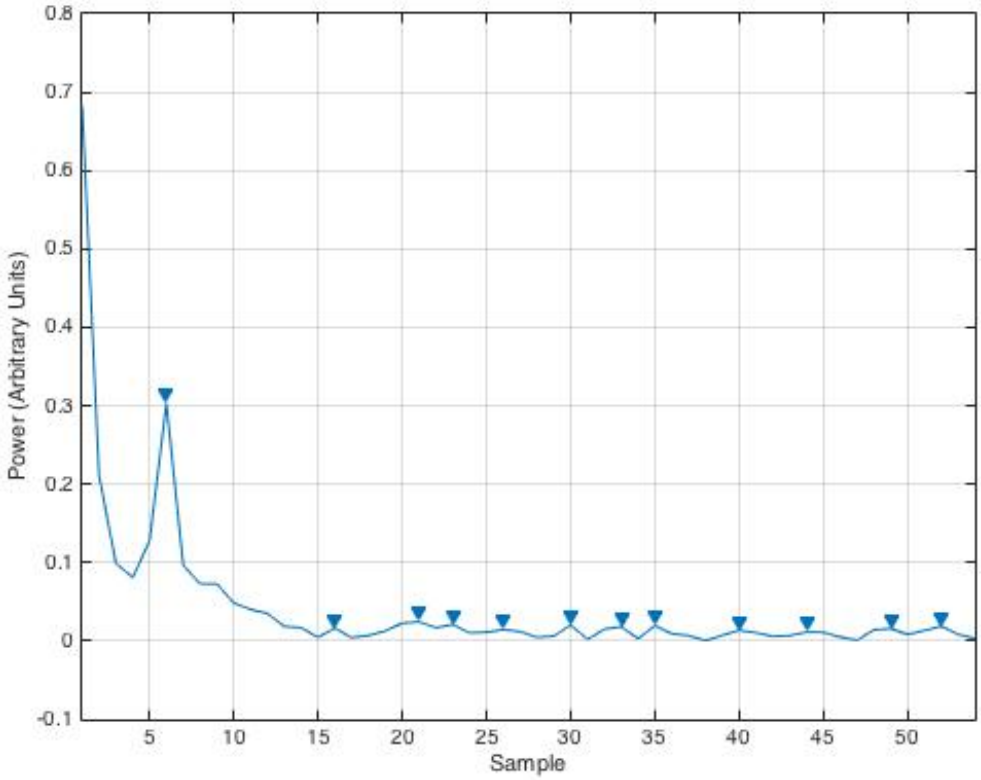

Figure X: FFT of the area forward of the two holes in the ITO layer (1.3 μm to 4 μm)

Figure X shows one blatantly obvious peak at sample number 6. This gives an interference frequency of 1.85 μm^{-1}. Upon inversion, this leads to a wavelength of 540 nm. This represents the interference pattern seen to the right of the two holes in the model in figure V.

4.4 Calculating Effective Indices

Knowing the interference wavelengths, it is possible to calculate the interference wavenumbers, and subsequently the effective indices of the ITO. In order to do this, the wavenumber must first be calculated using equation (7). Then, by a rearrangement of equation (11) for forward propagating waves, and equation (12)

for reverse propagating backscattered waves, the effective index (n_{eff}) can be found. The rearrangements result in,

$$n_{eff} = \frac{k_i \pm ksin\theta}{k}, \quad (16)$$

where the operator between k_i and $ksin\theta$ becomes positive for forward propagating waves, and negative for reverse propagating waves in the waveguide.

Single Hole			
Propagation	λ_i **(nm)**	k_i **(nm^{-1})**	n_{eff}
Backward **(Figure VII)**	141	0.0446	2.04
Forward **(Figure VIII)**	344, 460	0.0183, 0.0137	2.06, 1.76

Table II: Calculated wavenumbers and effective indices for both propagation directions for the single hole model

Two Holes			
Propagation	λ_i **(nm)**	k_i **(nm^{-1})**	n_{eff}
Backward **(Figure IX)**	152	0.0413	1.83
Forward **(Figure X)**	540	0.0116	1.63

Table III: Calculated wavenumbers and effective indices for both propagation directions for the two hole model

As seen in tables II above, the effective indices for the single hole model were 2.04 and 2.06, representing one mode, and 1.76 representing the second mode. This is in agreement with past research on similar ITO waveguides, which were experimentally confirmed using photoemission electron microscopy (PEEM) [10].

As seen in table III, the forward and backward propagations lead to slightly varying effective indices compared to the known results for ITO. This is due to the fact that the addition of a second hole leads to an interference pattern that is constructed of wave vectors that are no longer parallel to the line along which the data is collected. Therefore, to calculate the interference pattern, the incident light, the guided light, and the light intersecting from the two holes must be taken into account. This leads to a far more complex mathematical model. Although the mathematics involved are beyond the scope of this work, the two-hole model serves as a good indicator that simulations using COMSOL are helpful in displaying complicated experiments. This model may also serve as inspiration for further research.

Error in the results (although quite small) could possibly be attributed to the discrete nature of the FFT analysis method, as well as the fact that the sampling frequency employed by COMSOL was relatively low. These two issues combined lower the overall accuracy of the results by a small margin.

Chapter 5 – Conclusion

Through this research, characteristics of indium tin oxide waveguides were observed. Specifically in these two models, it was shown that several stable modes, and thus wavelengths, exist that support light wave propagation. It was shown that the wavelengths of the observed interference pattern differed drastically depending upon whether the light in the waveguide was propagating in the direction of the projection of the incident light upon the surface of the waveguide, or if it was

backscattered in the opposite direction. Through a Fourier analysis of the normalized electric field data taken from the models, the effective indices of the waveguides were calculated. The calculations are in agreement with previous research on similar ITO waveguides.

References

[1] Palais, Joseph C. Fiber optic communications. Englewood Cliffs: Prentice Hall, 1988.

[2] McNab, Sharee J., Nikolaj Moll, and Yurii A. Vlasov. "Ultra-low loss photonic integrated circuit with membrane-type photonic crystal waveguides." Optics express 11.22 (2003): 2927-2939.

[3] Dostalek, Jakub, et al. "Surface plasmon resonance biosensor based on integrated optical waveguide." Sensors and actuators B: Chemical 76.1 (2001): 8-12.

[4] Hunsperger, Robert G. *Integrated Optics: Theory and Technology*. Berlin: Springer, 1995, p. 26.

[5] Griffiths, David J. *Introduction to Electrodynamics*. 4th ed. London: Pearson, 2012, p. 393.

[6] Hunsperger, Robert G. *Integrated Optics: Theory and Technology*. Berlin: Springer, 1995, p. 19.

[7] Iizuka, Keigo. *Elements of Photonics*. New York, NY: Wiley-Interscience, 2002. p. 619

[8] Fitzgerald, J. P. S., Robert Campbell Word, and Rolf Könenkamp. "Subwavelength visualization of light in thin film waveguides with photoelectrons." Physical Review B 89.19 (2014): 195129.

[9] Watanabe, Koki, and Kousuke Kuto. "Numerical analysis of optical waveguides based on periodic Fourier transform." Progress In Electromagnetics Research 64 (2006): 1-21.

[10] Fitzgerald, J. P. S., Robert Campbell Word, and Rolf Könenkamp."Subwavelength visualization of light in thin film waveguides with photoelectrons." Physical Review B 89.19 (2014): 195129.